Addendum to ATBD

August 30, 2012

This addendum documents change made to the pre-launch version of ATBD through V1.3 of the algorithm which was implemented in April, 2012

I. Calibration

A. Initial Bias Adjustment

Immediately after the radiometers were turned on (August 25, 2011) a comparison was made between the expected antenna temperature, TA_exp, which is a prediction of the forward simulator and the actual measured antenna temperature, TA_mea. The two values, compared along an orbit as a function of time had the same shape and were separated by a small bias which gave us confidence in the accuracy of the simulator and proper functioning of the radiometers in space. The bias was within the error estimates for pre-launch calibration. It was decided to treat these "biases" as due to a gain error (which has been supported by several studies by S. Brown). An initial calibration of the radiometer was made by adjusting the pre-launch values of the internal noise diode (which in the calibration equations changes the gain and were determined by J. Piepmeier to be the primary contributor to pre-launch calibration uncertainty). The adjustments shown in the Table I were made and appeared in V1.1 of the code. The differences are within the reasonable range of adjustments (<14K) based on the pre-launch calibration uncertainty analysis (determined by analysis prior to launch).

Table I: Changes to Noise Diode Temperature (K)

	Radiometer Beam 1		Radiometer Beam 2		Radiometer Beam 3	
	V-Pol	H-Pol	V-Pol	H-Pol	V-Pol	H-Pol
Pre-Launch	652.40	670.93	673.53	690.75	724.15	681.61
V1.1	641.91	668.82	663.80	687.09	721.79	676.34
Difference	-10.49	-2.11	-9.73	-3.66	-2.3	-5.27

B. Gain Drift

The change described below has been tested is being implemented in V1.3.

When more data was available, it became apparent that the gain was slowly changing leading to a drift in TA_measured minus TA_expected of about 0.1 K per week. This was within radiometer performance specifications, but still significant in terms of the retrieved salinity. A root cause has yet to be determined although some manner of out-gassing is suspected, perhaps in the noise diode circuitry. Fig. I.B.1 illustrates the radiometer drift relative to the model (dTA = TA_measured minus TA_expected). There is clear evidence of both long term drift and shorter term non-monotonic fluctuations, some of which are likely due to the instrument.

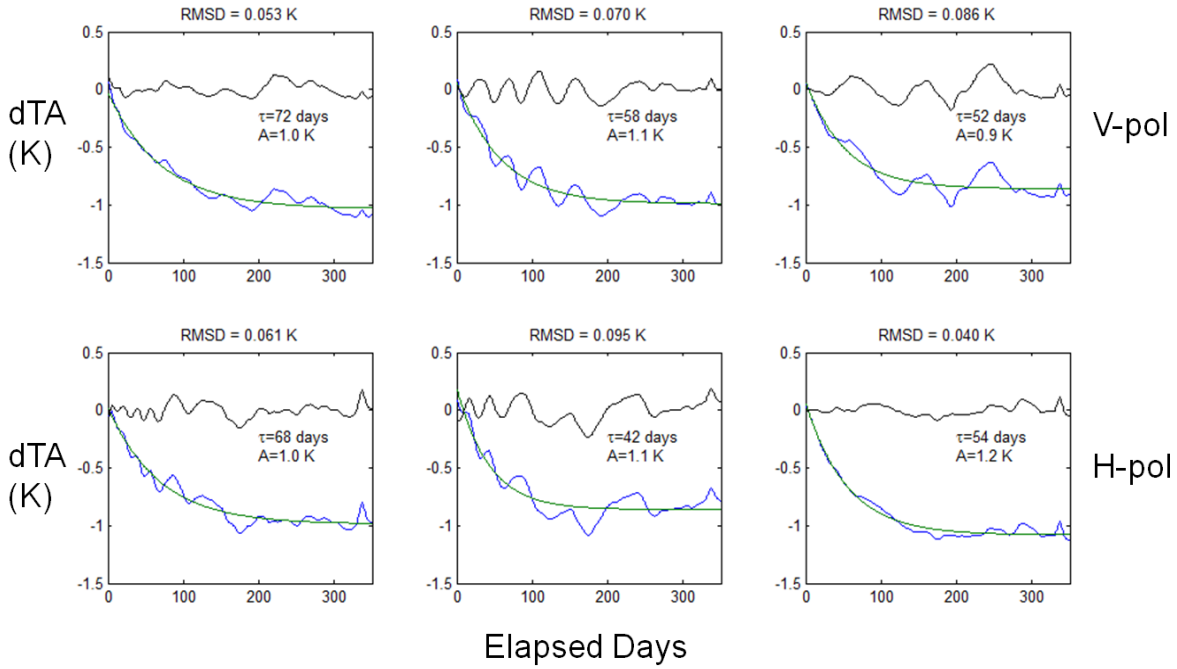

Figure I.B.1. Time series of TA_measured minus TA_expected for both polarizations of each beam (shown organized in columns from left to right) shown in blue for almost 1 year of observation. An exponential fit for each channel is shown in green and the residual is shown in black.

A model was developed to represent the change in terms of internal calibration references:

ND(ant)	=	Noise diode + antenna
ND(dl)	=	Noise diode + Dicke load
CND	=	Correlated noise diode

The measurements are expressed as ratios in order to cancel gain:

DR1	=	CND / ND(dl)	I.1
DR2	=	ND(ant) / ND(dl)	I.2

Then the change in antenna temperature is expressed as a linear combination of these deflection ratios. The form is based on a desire to keep the coefficients, K, comparable in magnitude and the model simple:

$$dTA = K0 + K1\ DR1 + 10\ K2\ [\ DR2 - 1] \qquad \text{I.3}$$

The calibration procedure is as follows:

1. The drift, dTA, is determined from data,TA_measured, and the simulator output, TA_expected.
   a. dTA = TA_measured - TA_expected;
   b. The DR1 and DR2 are determined from the calibration data;

c. All data since radiometer turn-on is used (but only over open ocean); Discussion is underway to further limit this data to reference sites where the ocean is relatively stable.

d. A minimum least square fit is used to determine the coefficients, K;

e. K's are updated weekly.

2. A change to the gain is made for each orbit

a. DR1 and DR2 are computed using the past 14 orbits (including the current orbit);

b. The new DR's are used in Equation I.1 to compute ΔTA;

c. An adjustment is made to the value of the noise diode:

- $T_{ND}^{new} = T_{ND}\ (1 - c)$, where $c = dT_A / (TA\_{expected} + dT_A - T_r)$;
- T_r is the brightness temperature of the reference Dicke load but the physical temperature T_0 is used instead as a close approximation;
- $[TA\_{expected} + dT_A]$ is computed using the mid-point of a linear fit to 15 orbits centered at the current orbit
- c is stored in the L2 science data file.

Figure I.B.2 illustrates the procedure and how it is integrated into the flow of the overall processing algorithm.

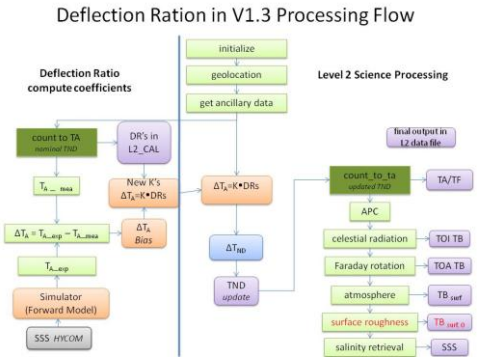

Figure I.B.2. Flow diagram illustrating how the deflection ratio is computed.

C. Unresolved Issues

1. Small gain "wiggles": The procedure above initial dealt with both the small wiggles and slow drift. Although it continues to address the slow drift, its performance with respect to thesmall wiggles on the mean has degraded and the variations remain.

2. Calibration of the third Stokes channel has yet to be addressed, although radiometer gain errors of the size observed on V and H polarizations (<1%) are unlikely to cause significant third Stokes errors. For example, a 1% error on T3=10 K is only 0.1K, which would result in a Faraday rotation correction error in V-pol of ~0.01 K .

3. Ascending/descending biases remain and are as yet unexplained.

4. Definitive assignment to errors in TA_measured minus TA_expected to either the instrument or model.

II. Antenna Pattern Correction, APC

The pre-launch A-matrix was based on simulations using the antenna patterns derived from the scale model. It was apparent almost immediately after launch that this resulted in too much cross-polarization coupling for the 1st and 2nd Stokes parameter into the 3rd Stokes parameter leading to unphysical values for the 3rd Stokes parameter. The A-matrix was revised based partly on the original theoretical antenna patterns (i.e. computed using byJPL using TICRA's GRASP software) and empirical adjustments that were required to obtain realistic values for the 3rd Stokes parameter The A-matrix was changed this one time and implemented in V1.1. This updated matrix is currently still being used in V1.3. Its elements are given below:

A. Original A-matrix

The Pre-Launch inverse APC Matrix A^{-1}

Radiometer Beam 1		
0.97087	0.01684	-0.02718
-0.00010	0.92868	-0.05440
-0.01381	0.05498	0.92870
Radiometer Beam 2		
0.967434	0.1414	-0.02700
-0.00062	0.94139	0.01538
-0.01845	-0.01169	0.94168
Radiometer Beam 3		
0.95966	0.01785	-0.01658
-0.00186	0.95200	-0.03767
-0.01387	0.04364	0.95421

B. Current A-matrix (V1.3)

The Post-Launch inverse APC Matrix A^{-1} (V1.3)

Radiometer Beam 1		
0.97087	0.00000	0.00000
0.00000	0.92635	0.00000
0.00300	0.00000	0.95848
Radiometer Beam 2		
0.96734	0.00000	0.00000
0.00000	0.91095	0.00000
0.00000	0.00000	0.93824
Radiometer Beam 3		
0.95966	0.00000	0.00000
0.00000	0.89485	0.00000
0.00500	0.00000	0.90913

C. Comments:

New antenna patterns have been computed at JPL using an enhanced GRASP model and computers capable of including more of the spacecraft-antenna structure. Evaluation of these new patterns is underway.

The APC is defined with respect to the Stokes vectors, I,Q and U.

III. Roughness Correction (Section 2.3.3)

The approach outlined in Section 2.3.3 of the ATBD has been modified based on an updated surface roughness model [Meissner et al. 2012]. The revised procedure is outlined below

A. Surface Roughness Model: Harmonic Coefficients

Our new model for the wind induced emissivity has been developed post-launch based on actual Aquarius observations. As a first step, Aquarius surface brightness temperatures were collocated with surface wind speed and wind direction measurements from NCEP, SSMIS F17 and WindSat, from which the harmonic coefficients A_i, i=0,1,2 of the wind induced brightness temperature can be de derived:

$$\Delta T_{B,rough} = \Delta E_W(W, \varphi_r) \cdot T_S = A_0(W) + A_1(W) \cdot \cos(\varphi_r) + A_2(W) \cdot \cos(2\varphi_r) \quad \text{III.1}$$

where each Ai(W) is a 5th order polynomial in W. W is the surface wind speed, φ_r is the surface wind direction relative to the beam look direction (i.e. azimuth relative to the direction of the antenna boresight) and T_S is the sea surface temperature. The results for the 3 Aquarius horns are shown in **Error! Reference source not found.** and the corresponding coefficients of the polynomial are given in Appendix A. This allows performing a roughness correction based on auxiliary wind speed and wind direction fields from NCEP.

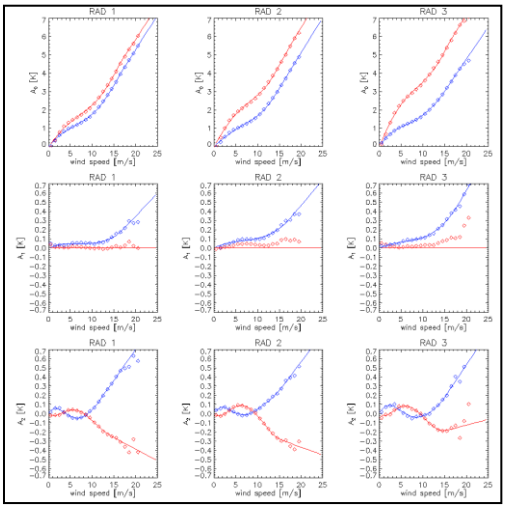

Figure III.1: Harmonic coefficients of the expansion **Error! Reference source not found.** of the wind induced surface brightness temperature $\Delta E_W \cdot T_S$ (in Kelvin) for the 3 Aquarius radiometers: blue = v-pol, red=h-pol.

These coefficients were determined using the historical data set (all of the Aquarius data from August 25 – December 31, 2011including ascending and descending passes).

B. Roughness and Scatterometer Backscatter

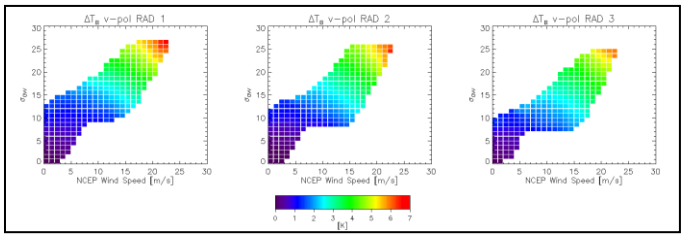

Figure III.2: The wind induced surface brightness temperature $\Delta E_W \cdot T_S$ [$\cdot$ 290 Kelvin] binned with respect to surface wind speed from NCEP W_{NCEP} and the scatterometer measurement $\sigma_{0,VV}$. The $\sigma_{0,VV}$ has been scaled to units of wind speed [m/s]. The wind direction signal has been removed from both $\Delta E_W \cdot T_S$ and $\sigma_{0,VV}$.

The goal is to use the radar backscatter cross section measurements, $\sigma_{0,}$ of the Aquarius scatterometer together with the NCEP wind speed and direction to improve the roughness correction. Both, radiometer and scatterometer observations are first corrected for wind direction. In the case of the radiometer, this is done using the NCEP wind direction in equation III.1 and subtracting the 1st and 2nd harmonic functions in equation III.1 from the TB. A function analogous to that given in equation 111.1 is used for the scatterometer $\sigma_{0.}$ The resultant wind induced brightness temperature and σ_0 are used to develop a look up table giving ΔTB_rough as a function of NCEP wind speed, $W_{NCEP,}$ and the σ_0 for the vv-pol backscatter. The results are shown in FigureIII.2.

C. The Roughness Correction Algorithm

The algorithm is illustrated in the flow diagram of Figure III.3.

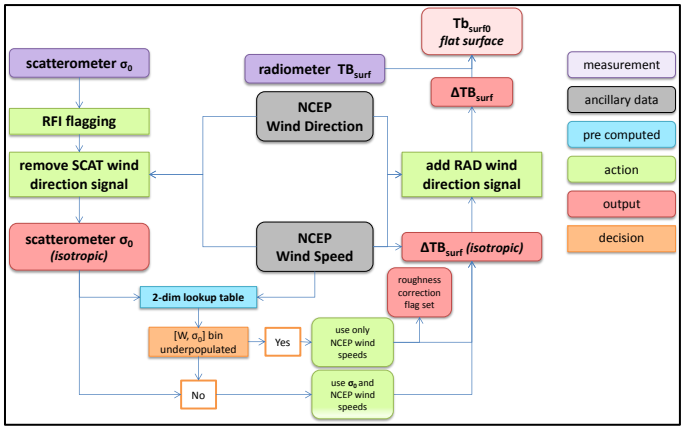

Figure III.3: Algorithm flow diagram for V1.3

The basis is the 2-dimensional look-up table from section III.B. First the scatterometer wind direction signal is removed from $\sigma_{0,VV}$. Its form is similar to the radiometer wind direction signal (equation III.1) and in order to compute it we use wind speed and wind direction from NCEP.

Then the value that is obtained from the look-up table as function of W_{NCEP} and the σ_{0VV} is used for computing the isotropic (wind direction independent) part of the roughness correction. The [W_{NCEP}, $\sigma_{0,VV}$] table is also associated with a histogram indicating the probability of occurrence of points in the 2-D graph. If the value associated with W_{NCEP} and $\sigma_{0,VV}$ falls outside bounds set for acceptable likelihood, then the A_0 coefficient in equation III.1 which is a function of W_{NCEP} only is used instead of the lookup table in order to compute the isotropic part. The same is done if the value for $\sigma_{0,VV}$ is unavailable or flagged as RFI contaminated. In both cases a roughness correction flag is set. Finally, the wind direction dependent part (1st and 2nd harmonic contribution in equation III.1) is added to obtain the complete surface roughness signal. For its computation we use again NCEP wind speed and direction.

D. Reflected and backscattered galactic, sun and moon radiation

No changes from the pre-launch version have been made in V1.3 for the computation of the reflected and backscattered celestial radiation terms (ATBD sections 2.2.2, 2.2.4, 2.2.6). As described in the ATBD, with the exception of the reflected component from the galaxy and sun glint (backscatter from the footprint into the main beam), no roughness correction is made for Rp. In particular, the reflectivity for a smooth "specular" surface is used for the reflected Sun and Moon. However, a correction is made for Earth curvature.

IV. Salinity Retrieval (Section 3.6)

Based on experience with Aquarius data, the procedure outlined in Section 3.6 (specifically Equations 54) has been modified.

In the current version, the effects of wind speed and direction are removed from TB_surf as outlined in Section III.C above. Best results were obtained using vertical polarization alone, and the data at horizontal polarization are currently not being used. Then salinity is retrieved from this roughness corrected surface TB at v-pol assuming a "flat" surface. That is, letting the roughness corrected brightness temperature be denoted by $T_{\_BE\_V\_surf\_0}$, one has:_

$$T_{\_BE\_V\_surf\_0} = T_{\_BE\_V\_surf} - T_{\_BE\_V\_rough}$$

$$= (1 - R_{V0})\, T_S \qquad \text{IV.1}$$

Where R_{V0} is the value of reflectivity at vertical polarization for a flat (specular) surface obtained from the Fresnel equations for the surface. The salinity retrieval consists in matching the value for $T_{BE\ V\ surf\ 0}$ obtained from Aquarius with the theoretical value for a specular surface shown in Equation IV.1. In the calculation of the reflectivity the Meissner-Wentz model for the dielectric constant of sea water at L-band is used *[Meissner and Wentz, 2004, 2012]*. Equation IV.1 can be solved for salinity numerically using a standard Newton iteration procedure It has been found that in a very rare instance that this Newton iteration does not converge. In this case, the algorithm for the salinity retrieval outputs a missing value.

VI. Algorithm Flow Diagram

Figure VII.1 illustrates the salinity retrieval code as implemented in V1.3. The process begins with the raw radiometer data ("Radiometer Counts"). These are filtered for RFI and then converted to calibrated brightness temperature (see Section I.B above) and averaged to form blocks of 1.44 sec. The result is "Total Antenna Temperature" called $T_{A,mea}$ in the ATBD. From this, the space contribution and the direct radiation from the Sun and Galaxy are removed. Also removed at this point are the reflected radiation from the Sun (reflected and glint), reflected radiation from the Galaxy, and a contribution from the Moon when it is near the main beam. Some of these terms require a correction for Faraday rotation as described in Section 2.2.2 of the ATBD .

The residual is the radiation from the Earth surface (Earth Antenna Temperature) called $T_{A\_earth\_dir}$ in the ATBD. This is then converted to a brightness temperature using the antenna pattern correction (APC) to yield a brightness temperature at the top of the ionosphere (TOI). This is corrected for Faraday rotation (Eqn 47) to yield the brightness temperature at the top of the atmosphere (TOA) called $T_{BE,toa}$ in the ATBD.

The next steps are to remove the effects of the atmosphere (upwelling and reflected downwelling radiation plus the constant contribution from the cosmic background). This is Equation 52 in the ATBD. The residual, $T_{B\ sur}$ is corrected for roughness as described above. The result represents the brightness temperature of an equivalent "flat" surface. Salinity is retrieved from this brightness temperature using only vertical polarization and assuming the Meissner-Wentz model for the dielectric constant of sea water at L-band.

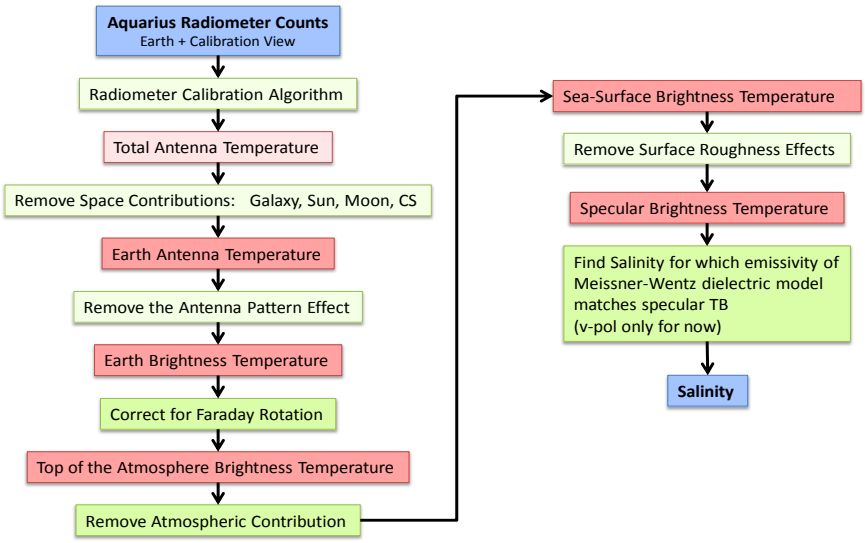

Figure VII.1: Schematic flow of the salinity retrieval algorithm.

Appendix A
Tables of Coefficients for Roughness Correction: Equation III.1

Beam 1: Vertical Polarization

n	A0	A1	A2
1	2.87E-01	2.18E-02	8.78E-02
2	-1.93E-02	-3.19E-03	-3.95E-02
3	-4.51E-04	1.53E-04	5.48E-03
4	1.88E-04	0.00E+00	-2.92E-04
5	-6.09E-06	0.00E+00	5.55E-06

Beam 1: Horizontal Polarization

n	A0	A1	A2
1	3.05E-01	0.00E+00	-4.87E-02
2	6.94E-03	0.00E+00	2.80E-02
3	-4.93E-03	0.00E+00	-4.57E-03
4	4.64E-04	0.00E+00	2.74E-04
5	-1.19E-05	0.00E+00	-5.69E-06

Beam 2: Vertical Polarization

n	A0	A1	A2
1	2.05E-01	2.37E-02	9.64E-02
2	7.19E-03	-2.69E-03	-4.01E-02
3	-3.69E-03	1.37E-04	5.69E-03
4	3.48E-04	0.00E+00	-3.30E-04
5	-8.86E-06	0.00E+00	7.00E-06

Beam 2: Horizontal Polarization

n	A0	A1	A2
1	3.98E-01	0.00E+00	-4.92E-02
2	1.22E-02	0.00E+00	2.95E-02
3	-6.82E-03	0.00E+00	-4.34E-03
4	5.83E-04	0.00E+00	2.25E-04
5	-1.42E-05	0.00E+00	-3.81E-06

Beam 3: Vertical Polarization

n	A0	A1	A2
1	3.68E-01	2.12E-02	1.01E-01
2	-4.26E-02	-2.55E-03	-3.45E-02
3	2.32E-03	1.57E-04	3.95E-03
4	2.03E-05	0.00E+00	-1.88E-04
5	-2.33E-06	0.00E+00	3.43E-06

Beam 3: Horizontal Polarization

n	A0	A1	A2
1	5.35E-01	0.00E+00	-5.17E-02
2	8.62E-03	0.00E+00	3.25E-02
3	-7.63E-03	0.00E+00	-5.15E-03
4	6.51E-04	0.00E+00	2.96E-04
5	-1.58E-05	0.00E+00	-5.67E-06